48.0   GRAIN BOUNDARY FRACTURE ANALYSIS IN ALUMINUM

Scott Blazanin (ISU)
Faculty: Pete Collins (ISU)
Industrial Mentor: Matt Krug (AFRL)

This project was initiated in November 2020 and is being supported by the Air Force Research Laboratory (AFRL) with industrial mentorship provided by Matt Krug. The research performed during this project will serve as a basis for the M.S. thesis project for Scott Blazanin.

48.1   Project Overview and Industrial Relevance

The demand for lighter, faster, and stronger aircraft has begun to push existing material-geometry combinations to their design limits. Over 95% of structural aircraft parts are made from aluminum and titanium alloys and polymer matrix composites [48.1]. Of these, aluminum alloys have often been a dominant choice owing to their good corrosion resistance, high specific strength, damage tolerance, and matured processing and inspection technologies [48.2]. In addition to material improvements, design changes have been made to enable the manufacture of single component structural supports such as bulkheads and wing spars. This part geometry shows improved performance and reduced weight compared to multi-component parts but must be manufactured from a single thick sheet of material [48.3].

To meet market demand for an improved aluminum alloy with good thick section properties in airframe components, Alcoa developed AA7085 (Al 7085), as a wrought alloy typically composed of (wt%) 7-8 Zn, 1.2-1.8 Mg, 1.3-2 Cu, 0.08-0.15 Zr, 0.08 Fe, 0.06 Si, and balanced with Al [48.4]. This alloy, offered as an upgrade to AA7075, is now being used in primary structural components in the Airbus A380 and Joint Strike Fighter aircrafts [48.2]. When compared to other alloys of the 7xxx series, AA7085 has superior thick section mechanical properties, quench insensitivity, fracture toughness, and fatigue properties while maintaining high specific strength and corrosion resistance [48.4]. Despite advantages over previous generations of aluminum alloys, Al 7085 has shown atypical crack growth behavior under cyclic loading [48.5], which has raised concerns over its viability as a material for structural components in aircrafts. Prior investigations have shown that forged components with certain grain orientations exhibit fatigue cracking behavior resulting in grain boundary delamination and unpredictable crack branching [48.5].

An understanding of the crack branching and grain boundary delamination behavior observed in cyclically loaded Al 7085 may allow for wider application of this material within the aerospace industry. With further characterization and analysis of the fatigue crack growth behavior, improvements can be made to lifecycle predictions and component maintenance for this material.

48.2   Previous Work

48.2.1   Literature Review

Neely studied the fatigue crack growth behavior in Al 7085 plates with different grain orientations, showing that critical stress intensities for crack deviation could be determined using standard testing practices [48.5]. Fatigue testing determined that drops in the stress intensity during fatigue crack propagation correlated with crack deviation from the primary crack direction. Additionally, the severity of crack branching was suggested to be a function of the applied load ratio, with higher load ratios showing more crack bifurcation events [48.5]. It should be noted that the scope of Neely's work does not include a discussion of subsurface crack propagation and that any subsurface damage was only discovered after testing to failure. Macroscopic crack branching events were observed on plate surfaces after cracks had progressed through the thickness of the specimens during testing. Some surface crack deviation events were photographed synchronously with fatigue testing, allowing for stress intensity factors to be paired with pictures of surface crack observations.

Microstructural effects on crack deflection and delamination fractures in varying compositions of aluminum alloys have been widely studied. Rao and Ritchie investigated the effects of microstructure on the mechanical properties

and fatigue crack propagation in second generation Al-Li alloys [48.6] and determined that grain anisotropy is a critical factor in determining fracture toughness. As shown in **Figures 48.1** and **48.2**, the primary crack can interact with the anisotropic grain structure in three different ways [48.6]. Firstly, in longitudinal transverse (L-T or T-L) loading, crack growth occurs transversely across grains. Secondly, in transverse short (T-S or L-S) loading, the crack is arrested by grain boundaries aligned perpendicular to the direction of primary crack growth. Lastly, for short longitudinal (S-T or S-L) loading, crack growth progresses through elongated grain boundaries leading to delamination cracking. The fracture toughness of specimens in delamination cracking orientations (S-L or S-T) was determined to exhibit half the fracture toughness of L-T and T-L orientations, and almost a quarter of the fracture toughness of the T-S orientation [48.6].

In addition to plate orientation, Rao and Ritchie showed that the strength and fracture toughness properties of Al-Li alloys were also dependent on precipitate dispersion in the microstructure. Superior strength and toughness combinations observed in alloys were primarily attributed to high volume fractions of coherent, strengthening precipitates throughout the matrix and minimal precipitation along grain boundaries [48.6, 48.7]. Indeed, the interaction of matrix and grain boundary precipitates in addition to plate orientation plays a critical role in delamination cracking events.

Grain boundary characteristics are shown to have a strong effect on crack behavior in laminated aluminum alloys. In Al-Li alloy 2090 forged plate samples, Tayon et al. found that delamination cracking depends on grain boundary characteristics, with brass textured grains of high misorientation presenting increased delamination cracking events [48.8]. Further EBSD analysis of neighboring grains that underwent delamination fracture indicated that a large Taylor factor difference in brass-textured grain pairs reliably showed delamination cracking. Large plastic deformation was observed to occur in grains along one edge of a delamination boundary, with local deformation accumulating in grains with low Taylor factors [48.8]. This study supports [48.8] the hypothesis that high energy grain boundaries and lack of accommodation for local slip correlate with increased delamination cracking events in aluminum alloys.

48.2.2   Sample Reception and Documentation

A sample set was received from the AFRL. The samples are the same plates that Neely used in his study of stress intensity factors and crack deviation in Al 7085 [48.5]. All specimens had middle-cracked fatigue test geometries and were extracted from hand forged plate. According to ASTM specification E399, for specimens extracted from a plate the geometry has to be related to the processing [48.9]. Specimen orientation is determined by two geometric designations separated by a hyphen. The first designation refers to the loading direction as tested, the second refers to the direction of primary crack growth. A diagram showing these orientations is given in **Figure 48.2**. Longitudinal-short transverse (L-S) and long transverse-short transverse (T-S) grain orientations were selected as they exhibited the greatest grain boundary delamination and crack deflection [48.5]. For each middle-cracked, hand forged specimen, stress ratios (R) of 0.1, 0.9, and -0.7 were selected. An overview of the sample set is provided in **Table 48.1**. Macroscale images of the as-tested plates can be seen in **Figure 48.3(a-f)**.

A system has been implemented to carefully track changes made to the received specimens. Each specimen was photo-documented and clearly labelled to show the processing orientation. Additionally, an inventory of received samples has been created and will be updated as further experimentation commences. Excised samples from as-tested plates will follow a naming scheme that allows them to be easily traced to their parent sample. For data management and curation, records will be kept on Microsoft OneDrive and shared with both academic and industry mentors.

48.3   Recent Progress

48.3.1   Fracture Edge Stereomicrograph Mosaics

The received sample set was imaged using stereomicroscopy for the purposes of creating fracture edge image mosaics and obtaining higher magnification photo-documentation of plate specimens in the as-tested condition. As shown in **Figure 48.4**, the full fracture edge was imaged at a resolution sufficient to identify secondary cracks

emerging from the plate surface. For each plate specimen, a minimum of 65 stereomicrographs were taken along each fracture edge and include the full length of primary cracking and approximately 3 centimeters of surrounding plate material along each edge.

48.3.2 Sample Sectioning

All six plate specimens were sent off-site for electrical discharge machine (EDM) sectioning. For each plate, four fracture edge specimens were excised for crack analysis, as well as one section far from the fracture edge for analysis of the base microstructure, as indicated in **Figure 48.5** for specimen MH-TS-07. Following EDM sectioning, through-thickness sectioning was performed just outside the centerline thickness via precision low-speed saw. This thickness was selected to allow for metallographic preparation approaching the centerline where crack network density is highest, as shown in **Figure 48.6**. Characterization of crack behavior and microstructural interactions will be conducted at centerline thickness, for all samples.

48.3.3 Development of a Metallographic Preparation Procedure

In collaboration with scientists at the Air Force Research Laboratory, a procedure was developed for the metallographic preparation of Al 7085. This procedure, outlined in **Table 48.2**, is optimized for edge retention and sample cleanliness, both of which are required for accurate indexing of fracture edge grains via EBSD. Extra care is taken to minimize induced surface deformation and the avoid delamination crack widening through corrosion or electrolytic processes.

48.4 Plans for Next Reporting Period

- SEM analysis of crack behavior and microstructural effects on crack growth.
- EBSD texture analysis of near-fracture surfaces for L-S and T-S orientations.
- Pair crack growth and grain boundary delamination metrics with stress intensity data established by Neely.

48.5 References

[48.1]   I.J. Polmear, Recent Developments in Light Alloys, Materials Transactions, JIM. 37 (1996) 12–31. doi:10.2320/matertrans1989.37.12.

[48.2]   T.R. Prabhu, An Overview of High-Performance Aircraft Structural Al Alloy-AA7085, Acta Metallurgica Sinica (English Letters). 28 (2015) 909–921. doi:10.1007/s40195-015-0275-z.

[48.3]   J.T. Burns, J. Boselli, Effect of plate thickness on the environmental fatigue crack growth behavior of AA7085-T7451, International Journal of Fatigue. 83 (2015) 253–268. doi:10.1016/j.ijfatigue.2015.10.020.

[48.4]   L. Mueller, L. Suffredini, D. Bush, ALCOA 7085 Forgings: 7th Generation Structural Solutions, 1130cc.Com. (2006). https://www.1130cc.com/forums/attachment.php?attachmentid=485073&d=1471292095 (accessed March 19, 2021).

[48.5]   J.A. Neely, Correlation of stress intensity range with deviation of the crack front from the primary crack plane in both hand and die forged aluminum 7085-T7452., thesis, 2019.

[48.6]   K.T. Venkateswara Rao, R.O. Ritchie, Mechanical properties of Al–Li alloys Part 1 Fracture toughness and microstructure, Materials Science and Technology. 5 (1989) 882–895. doi:10.1179/mst.1989.5.9.882.

[48.7]   K.T. Venkateswara Rao, R.O. Ritchie, Mechanical properties of Al–Li alloys Part 2 Fatigue crack propagation, Materials Science and Technology. 5 (1989) 896–907. doi:10.1179/mst.1989.5.9.896.

[48.8]   W. Tayon, R. Crooks, M. Domack, J. Wagner, A.A. Elmustafa, EBSD study of delamination fracture in Al–Li alloy 2090, Experimental Mechanics. 50 (2008) 135–143. doi:10.1007/s11340-008-9202-9.

[48.9]   E399-20a Standard Test Method for Linear-Elastic Plane-Strain Fracture Toughness of Metallic Materials, ASTM Compass. (2021). https://doi.org/10.1520/E0399-20A (accessed March 19, 2021).

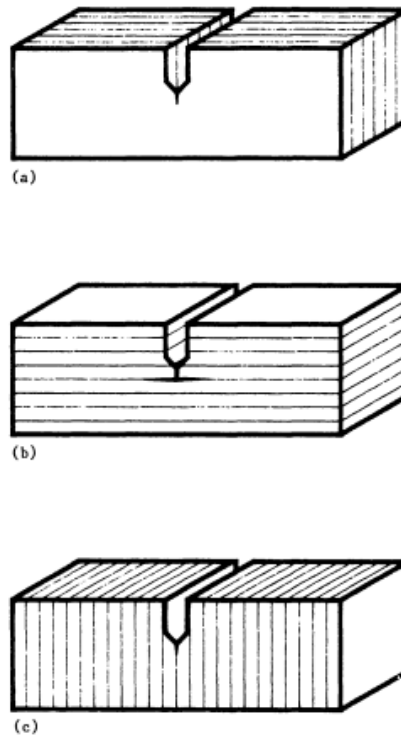**48.6   Figures and Tables**

Figure 48.1: Schematic of orientations for crack extension in anisotropic material containing specific planes in one direction; (a) crack dividing orientation corresponding to L-T and T-L, (b) crack arresting orientation corresponding to T-S and L-S, (c) crack delamination orientation corresponding to S-L and S-T [48.6].
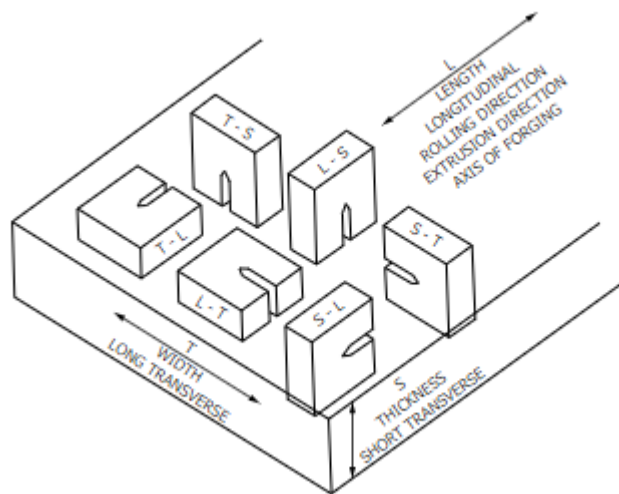

Figure 48.2: Schematic showing different orientations of test specimens that can be excised from a plate [48.9]. For each specimen orientation, the first letter represents the test loading direction while the second letter describes the direction of primary crack growth with respect to the plate. For example, S-L corresponds to a specimen pulled along the thickness of the plate with a primary crack propagating in the longitudinal direction of the plate.
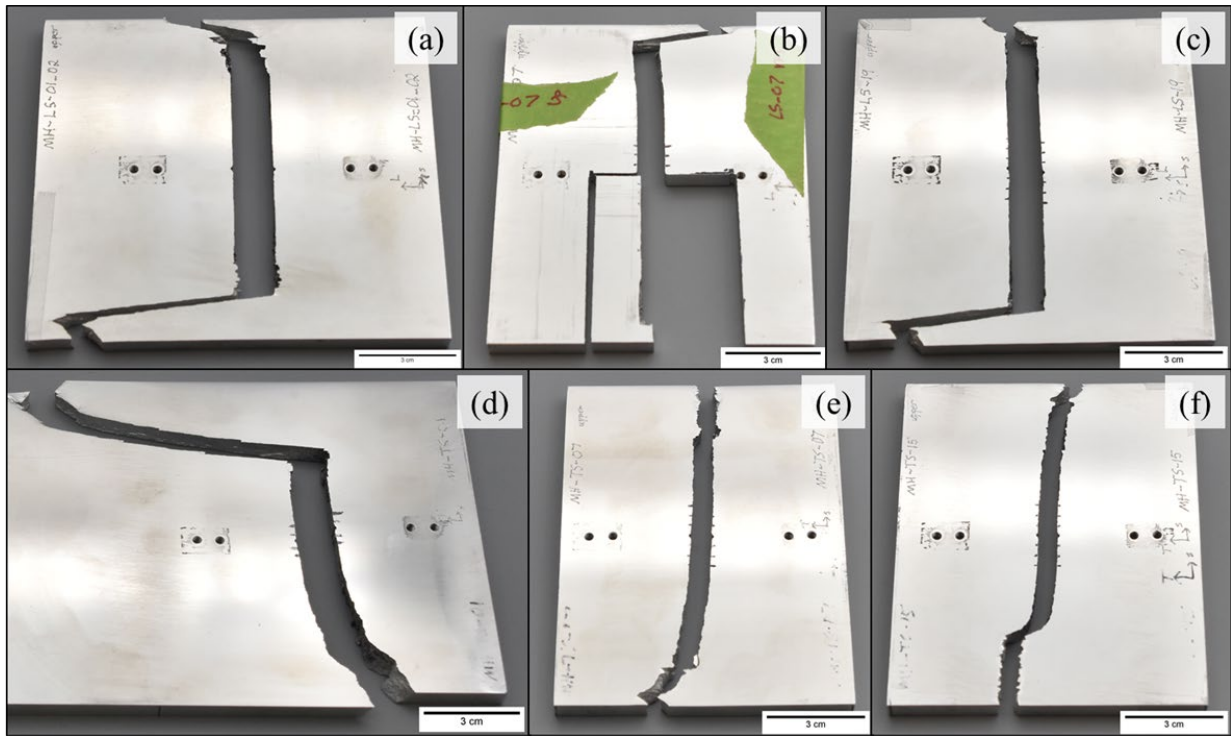
48.4

Figure 48.3: Macroscale images of as-tested Al 7085 plate specimens. (a) Specimen MH-LS-01_02, (b) MH-LS-07, (c) MH-LS-19, (d) MH-TS-01, (e) MH-TS-07, (f) MH-TS-19.

Table 48.1: Sample set received from AFRL. The table provides a description of specimen identity, history, and testing conditions. Companion macroscale images are referred to in **Figure 48.3**.

Specimen Name	Grain Orientation	Load Ratio	Image
MH-LS-01_02	L-S	0.1	Figure 48.3a
MH-LS-07	L-S	0.7	Figure 48.3b
MH-LS-19	L-S	-0.9	Figure 48.3c
MH-TS-01	T-S	0.1	Figure 48.3d
MH-TS-07	T-S	0.7	Figure 48.3e
MH-TS-19	T-S	-0.9	Figure 48.3f

48.5

Figure 48.4: Image mosaic from stereomicrographs along the full fracture edge of plate MH-LS-01.
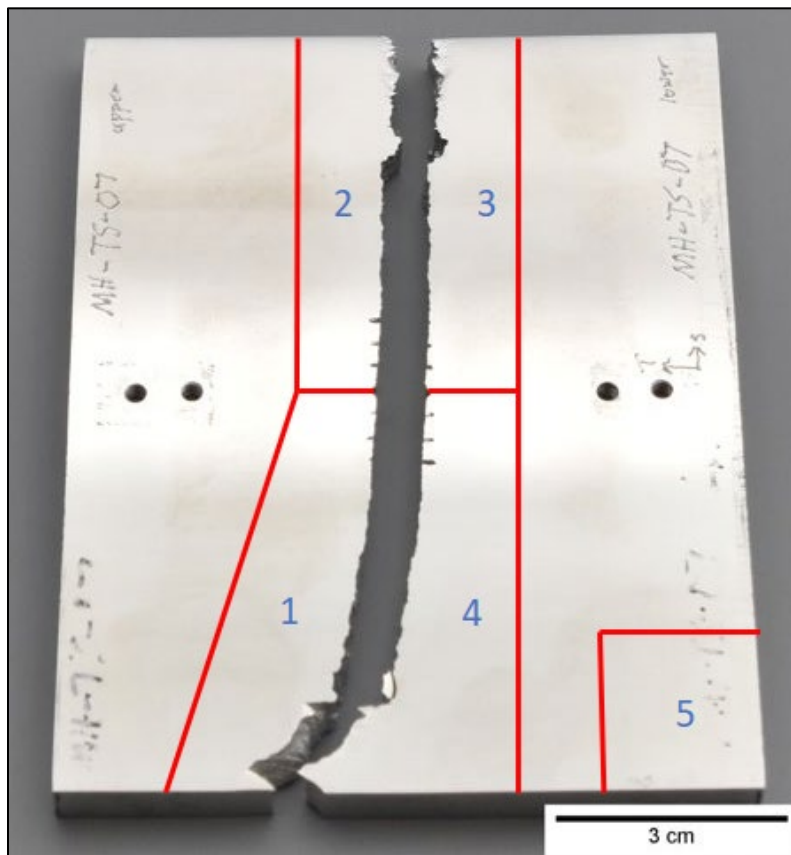
48.6

Figure 48.5: Machining instructions for EDM sectioning of center-cracked panel MH-TS-07. Sectioning will result in four fracture edge specimens (numbered 1-4) and one base microstructure specimen (number 5) for each plate.
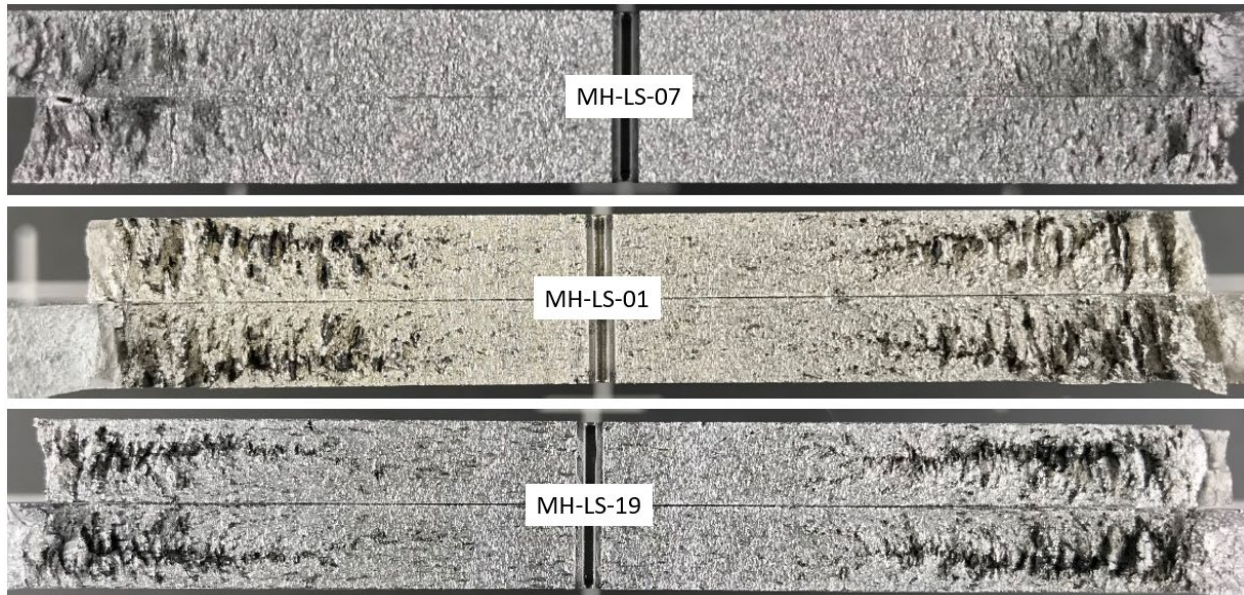

Figure 48.6: Fracture surface images of L-S orientation plates following fatigue testing. Secondary crack networks are observed to have the highest crack density near the centerline thickness for each plate.

Table 48.2: Overview of the preparation procedure for EBSD analysis of Al 7085 fracture specimens.

Step	Description
1	Mounting in long cure epoxy with vacuum impregnation
2	400 grit grinding to establish plane
3	600 grit grinding for damage removal
4	1200 grit fine grinding
5	3 μm and 1 μm diamond polishing
6	0.05 μm colloidal silica polishing
7	0.05 μm colloidal silica vibratory polishing
8	Final cleaning, drying, and mounting for SEM/EBSD